Atmos. Chem. Phys. Discuss., 10, 10077–10112, 2010
www.atmos-chem-phys-discuss.net/10/10077/2010/

Atmospheric Chemistry and Physics Discussions

This discussion paper is/has been under review for the journal Atmospheric Chemistry and Physics (ACP). Please refer to the corresponding final paper in ACP if available.

Chemical transformations of Hg° during Arctic mercury depletion events sampled from the NASA DC-8

S. Y. Kim[1], R. Talbot[1], H. Mao[1], D. R. Blake[2], G. Huey[3], and A. J. Weinheimer[4]

[1]Climate Change Research Center, Institute for the Study of Earth, Oceans, and Space, University of New Hampshire, Morse Hall, Durham, NH 03824, USA
[2]Department of Chemistry, University of California – Irvine, Irvine, California 92697-2025, USA
[3]School of Earth & Atmospheric Sciences, Georgia Institute of Technology, Atlanta, GA 30332, USA
[4]National Center for Atmospheric Research, Earth and Sun Systems Laboratory, P.O. Box 3000, Boulder, Colorado 80307-3000, USA

Received: 1 March 2010 – Accepted: 1 April 2010 – Published: 16 April 2010

Correspondence to: S. Y. Kim (sk@gust.sr.unh.edu)

Published by Copernicus Publications on behalf of the European Geosciences Union.

Abstract

Atmospheric Mercury Depletion Events (MDEs) in Arctic springtime were investigated utilizing a box model based on airborne measurements from the NASA DC-8 during the Arctic Research of the Composition of the Troposphere from Aircraft and Satellites (ARCTAS) field campaign. Measurements showed that MDEs occurred near the surface and always over the Arctic Ocean accompanied by concurrent ozone (O_3) depletion, enhancement in Br_2 mixing ratios, and decreases in ethyne and light weight alkanes. Backward trajectories indicated that most air masses inside the MDEs originated at low altitude over the ocean presumably generating a halogen-rich environment. We developed a box model which considered only gas phase reactions of mercury, halogen species, and O_3 chemistry. We conducted a series of sensitivity simulations to determine the factors that are of most importance to MDE formation. The box model results suggested that continuous enhancement of Br_2 mixing ratios, a high intensity of solar radiation, or a relatively high NO_x regime expedited Hg° depletion. These environments generated high concentrations of Br radical, and thus the model results indicated that the Br radical was very important for Hg° depletion. Utilizing different rate constants for reaction of $Hg^\circ + Br$ produced times to reach Hg° depletion ranging from 22 to 32 h.

1 Introduction

Atmospheric mercury exists in three forms, gaseous elemental mercury (Hg°), reactive gaseous mercury (RGM), and particulate mercury (PHg). Hg° comprises ~95% of total gaseous mercury (TGM = Hg° + RGM) in the atmosphere (Lin and Pehkonen, 1999; Malcolm et al., 2003; Poissant et al., 2005). Atmospheric mercury that enters terrestrial and aquatic ecosystems (Branfireun et al., 2005; Magarelli and Fostier, 2005; Strode et al., 2007) can be subsequently transformed to organic mercury (e.g., methyl mercury) (Branfireun et al., 2005). Organic and inorganic mercury are harmful to humans

ACPD

10, 10077–10112, 2010

through food chain uptake; they are thus categorized as toxic compounds by the US Environmental Protection Agency.

Atmospheric mercury depletion events (MDEs) have been observed near the surface in the Arctic springtime. Schroeder et al. (1998) were the first to observe that TGM values, which were 1–2 ng m^{-3} in winter, dropped off to <1 ng m^{-3} after mid-March at a Canadian Arctic site. Strong positive correlation between Hg° and O_3 was found in springtime air masses originating from the Arctic (Eneroth et al., 2007; Lu et al., 2001). In addition, MDEs in interstitial air of snowfall, where Hg° concentration was decreased from 5 to 0.4 ng m^{-3}, was found at about 1 m depth in the snowpack at the Kongsvegen Glacier, 10 km south-east from Ny Ålesund, Svalbard (Fain et al., 2006).

Atmospheric mercury depletion in the Arctic has been attributed to meteorological and chemical processes. The strong near-surface inversion layer during winter and early spring creates a vertically isolated thin boundary layer over the Arctic, and it plays an important role in the occurrence of MDEs by blocking re-supply of atmospheric chemical species such as O_3 and Hg° from the free troposphere (Lehrer et al., 2004). Chemically, the occurrence of MDEs could be closely related with the transformation of Hg° to RGM and PHg as a result of its oxidation by reactive halogen radicals which are likely abundant after polar sunrise (e.g., Cobbett et al., 2007; Lindberg et al., 2002). RGM easily deposits to the surface of aerosols due to its high water solubility (Lin and Pehkonen, 1999) to form PHg. Both RGM and PHg can be removed from the atmosphere relatively quickly due to their high dry deposition velocities (Schroeder and Munthe, 1998).

Box model studies suggest that reactive bromine compounds (e.g., Br and BrO) are much more important for the occurrence of MDEs than chlorine and sulfur compounds (Ariya et al., 2004; Calvert and Lindberg, 2003; Goodsite et al., 2004; Xie et al., 2008). It was speculated that highly reactive bromines are derived mainly from the surface sea ice and less reactive bromines, such as HBr, are from sea salt aerosols (Lehrer et al., 2004). As a result of mercury oxidation, a few studies suggested that the most abundant RGM chemical compounds would be HgO, $HgBr_2$, and BrHgOBr formed by

reaction of Hg° with bromine radical (Calvert and Lindberg, 2003; Xie et al., 2008).

The Arctic Research of the Composition of the Troposphere from Aircraft and Satellites (ARCTAS) field campaign, carried out by the National Aeronautics and Space Administration Tropospheric Chemistry Program, was conducted over 3 weeks each in April and July 2008 with focus on impacts on Arctic atmospheric composition from long-range transport of pollution, boreal forest fires, aerosol radiative forcing, and chemical processing. Here, we aimed to understand the chemical mechanisms driving the occurrence of MDEs in the Arctic spring using box model results based on extensive measurements of mercury and other chemical compounds from the NASA DC-8 aircraft during the 2008 April deployment.

2 Methods

2.1 ARCTAS measurement data

Hg° was measured with a time resolution of 2.5 min by the University of New Hampshire cold vapor atomic fluorescence spectrometer during the ARCTAS field campaign. We utilized a modified Tekran 24537A as described by Talbot et al. (2008). The limit of detection (LOD) of the instrument was ~0.2 ng m^{-3} (~22 ppqv). The internal pressure of the instrument was maintained during the analysis stage at 1100 hPa. In-flight zeroing and standard additions were conducted on all flights.

Ozone was measured at 1 Hz using the chemiluminescence technique as described in Ridley et al. (1992). The University of California at Irvine sampled using stainless steel passivated canisters to determine more than 75 gases including nonmethane hydrocarbons, halocarbons, alkyl nitrates and sulfur compounds. A comprehensive description of the sampling and analytical techniques can be found in Colman et al. (2001). The Georgia Institute of Technology chemical ionization mass spectrometer was used to measured BrO and Br_2 every 30 seconds using the reagent SF_6^-. A detailed explanation of the technique is given in Neuman et al. (2010). The University

ACPD
10, 10077–10112, 2010

of New Hampshire group collected aerosols on Teflon filters with subsequent analysis for soluble ions by ion chromatography (Dibb et al., 2003). This group also sampled water-soluble gases using the mist chamber technique (Scheuer et al., 2003).

There were 14 MDE cases below 5 km altitude in which the Hg° mixing ratio was depleted to <50 ppqv (1 ng m^{-3} = 112 ppqv). The spatial map of mixing ratios of Hg°<50 ppqv, O_3<10 ppbv and Br_2>2 pptv as observed during ARCTAS is displayed in Fig. 1. Eight cases exhibited generally distinct features of MDEs, i.e., the concurrence of high Br_2, low O_3, and low Hg° mixing ratios (Table 1), and these will be the focus of this study. It should be noted though that the mixing ratios of O_3 right at the onset and ending of the MDEs were mostly >10 ppbv. Case 6 showed O_3 values during the MDE that were close to 10 ppbv. Six cases did not show a concurrence of high Br_2, low O_3, and low Hg°. The comparison between these two types of cases should be interesting, but unfortunately we could not study the six non-concurrence cases due to a lack of sufficient measurement data. Perhaps these cases reflected the later stages of a MDE with the mixing of MDE air with other air masses.

2.2 Trajectories

Kinematic backward trajectories were provided at one minute time steps throughout ARCTAS by Florida State University (http://www-air.larc.nasa.gov/cgi-bin/arcstat-c). The three-dimensional wind components were utilized from the Weather Research and Forecasting (WRF) Model hourly output at 45 km resolution to calculate the backward trajectories (Fuelberg et al., 1996, 2000; Martin et al., 2003). For each MDE case, the corresponding five-day backward trajectories are shown in Fig. 2. The trajectories allowed comparison of air mass origins both outside and inside the MDE areas.

2.3 Box model description

Mercury gas phase reactions occur mainly with O_3, H_2O_2, halides such as Br_2, Cl_2, and radicals OH, Br, Cl, and I (Table A in the supplementary document, http://www.

atmos-chem-phys-discuss.net/10/10077/2010/acpd-10-10077-2010-supplement.pdf). The multitude of mercury chemical reactions and their rates are not clearly established yet. Differing results have been published on the products of some mercury chemical reactions. For example, the reaction between Hg° and OH apparently has two different products - HgOH and HgO (Goodsite et al., 2004; Sommar et al., 2001; Pal and Ariya, 2004a). Furthermore, values of the rate constant for many Hg° reactions vary considerably. There is large uncertainty in the rate constant of the reaction between Hg° and O_3, ranging from $3.0\times10^{-20}\,cm^3\,molecule^{-1}\,s^{-1}$ at 293 K (Hall, 1995) to $7.5\times10^{-19}\,cm^3\,molecule^{-1}\,s^{-1}$ at 298 K (Pal and Ariya, 2004b). Rate constants for Hg° reactions with halogen radicals that have been reported in literature also vary greatly. The rate constant of Hg° with Cl radical at 298 K ranges from $6.38\times10^{-13}\,cm^3\,molecule^{-1}\,s^{-1}$ (Donohoue et al., 2005) to $1.0\times10^{-11}\,cm^3\,molecule^{-1}\,s^{-1}$ (Ariya et al., 2002). Rate constants of Hg° reaction with Br vary from $4.23\times10^{-13}\,cm^3\,molecule^{-1}\,s^{-1}$ (Donohoue et al., 2006) to $3.2\times10^{-12}\,cm^3\,molecule^{-1}\,s^{-1}$ (Ariya et al., 2002). Finally, BrO is recognized as an important oxidant in Arctic mercury chemistry (Goodsite et al., 2004), but the rate constant values vary from 10^{-13} to $10^{-15}\,cm^3\,molecule^{-1}\,s^{-1}$ for its reaction with Hg° at a temperature of 298 K (Raofie and Ariya, 2003). We did not include this reaction in most cases except in Sect. 4.2 where the possible role of this reaction in the occurrence of MDEs was studied. Overall, our box model includes 28, 43, and 10 reactions for bromine, chlorine, and iodine chemistry respectively. In addition, there are 10 mercury gas phase reactions and 35 for O_3 chemistry (Table A–C in the supplementary document, http://www.atmos-chem-phys-discuss.net/10/10077/2010/acpd-10-10077-2010-supplement.pdf).

The Kinetic PreProcessor (KPP) version 2.1 is the basic model framework (Sandu and Sander, 2006), and it has been utilized to study mercury chemistry previously (Hedgecock et al., 2005; Pan and Carmichael, 2005). The structure solves ordinary differential equations, and we used a second order Rosenbrock method (Verwer et al., 1999). Ideal (i.e., theoretical) experiments were used to clearly identify how environ-

mental factors (e.g., photolysis) influenced Hg° or O_3 depletion. As shown in Section 3, backward trajectories for each case indicated that air masses were principally transported over short distances in the 24 h prior to airborne measurements. During the MDEs, cold CN concentrations were mainly <500 #/cm^3, which indicated low aerosol concentrations in the atmosphere, and air temperature averaged 255±5 K which was cold enough to freeze the ocean surface. Moreover, the water vapor mixing ratios were <1700 ppmv during MDEs period, which were low values, for example, compared to 7000–19 000 ppmv near the surface in the vicinity of Hawaii in the spring Intercontinental Chemical Transport Experiment – B field campaign. We examined the possibility of heterogeneous chemistry on the ice surface or in the aerosol. In the simplified mechanism of heterogeneous chemistry, there are three steps which are adsorption onto the aerosol or ice surface, diffusion into the bulk, and Henry's law equilibrium. Although temperature does not affect the transport velocity of a gas to the interface, diffusion into the bulk following the Einstein relation and Henry's coefficient are influenced considerably by temperature. In the meteorologically stable Arctic at 255 K it is reasonable to ignore horizontal and vertical transport, deposition, uptake by sea-salt aerosol, and aqueous phase reactions in the simulations. We only considered I_2, Br_2, and Cl_2 emissions from the ocean, and the mixing ratios for these species were set to constant values at each time step to simulate continuous emissions. We also did not consider daily and diel variation in photolysis rates.

Initial values in the simulations were taken from the ARCTAS measurements (Table 2). The data for several minutes were selected from outside the MDE regions for the eight cases and averaged to set the initial values. Photolysis rate constants were averaged for each MDE period, and the average values were categorized into three groups which were high, middle, and low values. The high values were a factor of 2 greater than middle values and the same pattern existed between the middle and low values (Table 3).

We conducted 14 ideal case sensitivity experiments using ARCTAS measurements. The base case used average initial concentrations and the middle value of the photol-

ysis rate constants (Table 2 and 3). In this base case run we utilized the rate constant from Pal and Ariya (2004a) for reaction of Hg° with OH, the rate constant from Goodsite et al. (2004) for reaction of Hg° with Br, the rate constant from Khalizov et al. (2003) for the Hg° + Cl reaction, and the rate constant from Ariya et al. (2002) for the Hg° + Br_2 reaction (Table A in the supplementary document, http://www.atmos-chem-phys-discuss.net/10/10077/2010/acpd-10-10077-2010-supplement.pdf). In four control runs, we utilized high and low photolysis rate constant values (Table 3), and high NO_x (5000 pptv NO and 900 pptv NO_2) and low NO_x (0.32 pptv NO and 0 pptv NO_2) regimes based on ARCTAS measurements. In five sensitivity runs different rate constants were used for mercury chemistry: (1) Goodsite et al. (2004) for the Hg° with OH reaction, (2) Khlaizov et al. (2003) and Donohoue et al. (2006) for the Hg° with Br reactions, (3) Balabanov et al. (2005) for the Hg° with Br_2 reaction, and (4) Donohoue et al. (2005) for the Hg° with Cl reaction (Table A in the supplementary document, http://www.atmos-chem-phys-discuss.net/10/10077/2010/acpd-10-10077-2010-supplement.pdf). In three control runs the sensitivity of mercury chemistry to varying mixing ratios of Br_2 and Cl_2 where studied using 3 and 5 pptv Br_2 and 5 pptv Cl_2 mixing ratios. One last control run was conducted without re-setting I_2, Cl_2, and Br_2 mixing ratios at each time step to their initial conditions to simulate no emission flux from the surface.

3 Characteristics of MDEs

General features of the eight MDEs can be summarized as follows. MDEs were found only near the surface over the ocean. We selected 3–10 points before and after the MDE time window to compare the geographical locations and the vertical extent of all MDEs, and we defined these data as outside the MDE. Hg° mixing ratios from this subset of data varied from 100 ppqv to 250 ppqv, and the corresponding O_3 mixing ratios were usually >30 ppbv. The principal pattern of variation in Hg° from outside to inside the MDE area is characterized by a precipitous fall from >100 ppqv to the

ACPD
10, 10077–10112, 2010

LOD, while in comparison O_3 decreased rather gradually from >30 ppbv to <10 ppbv. Four out of the eight cases showed a sudden Br_2 build-up up to 7 pptv inside the MDE areas. Ethyne mixing ratios also decreased during MDEs, and it was correlated with O_3 at $r^2 = 0.72$. Moreover, light alkanes such as C_2H_6, C_3H_8, C_4H_{10} and C_5H_{12} showed the same pattern of variation as that of C_2H_2. Similar findings were reported previously for O_3 depletion events (ODEs) (Mao et al., 2010; Eneroth et al., 2007). A general feature ascertained from backward trajectories was that air masses outside most MDEs originated from the mid-troposphere, whereas air masses inside MDEs traveled at low altitude over the ocean surface probably entraining halogen-rich chemical compounds. Analysis of variations in chemical compounds and backward trajectories indicated that halogen-rich air could be related to changes in Hg°, O_3, and light alkanes. In addition, fresh combustion emissions were sampled as evidenced by high NO_x levels in cases 3 and 8. The backward trajectories suggested that the high NO_x originated from unknown sources in northern Alaska.

Important chemical compounds in this study included Hg°, O_3, and Br_2, and the mixing ratios for each case are summarized in Table 1 and Figure 3. MDEs were sampled over horizontal distances of ~225 km (case 1), and it appeared to be a typical MDE case with distinct demarcations in the spatial series of chemical compounds (Table 1 and Fig. 3). Mixing ratios of Hg° decreased suddenly from >125 ppqv to the LOD except for one point of 22 ppqv. Ozone mixing ratios dropped quickly from ~50 ppbv to 0–6 ppbv during the same period. Mixing ratios of Br_2 varied between 3.2 pptv and 5.8 pptv, which are considerably higher than the values outside the MDE (0.05–1.8 pptv). Moreover, mist chamber collected water-soluble bromide also increased by ~20 pptv and bromide (Br^-) in aerosol phase by at least 3 pptv compared to values outside the MDE. However, 4 samples inside the MDE showed that chloride (Cl^-) in the aerosol phase decreased from 136 to 56 pptv. Mixing ratios of CH_3Cl, CH_3Br, and CH_3I did not show any discernable changes. Light alkanes and C_2H_2 tracked changes in Hg° and O_3 closely. For example, C_2H_6 mixing ratios decreased by ~700 pptv from outside to inside the MDE areas.

Backward trajectories for case 1 indicated that the air masses captured in the airborne measurements over the MDE area mostly originated from Nunavut at low altitude traveling off the shore of northern Greenland for 24 h prior to the measurements. Some air masses during the MDE period traveled at the 850–650 hPa surfaces from southwestern Greenland. In comparison, air masses outside the MDE were transported on 850–500 hPa surfaces from Nunavut or from southwestern Greenland at altitudes ranging from near the surface to 700 hPa.

Case 2 followed case 1 a day later occurring over a similar geographical area around the similar time of the day (~13:00 local time). However, backward trajectories for case 2 suggested that air masses originated from the Baffin Bay area in the mid-troposphere, and were transported to the sampling location through northern Nunavut at near-surface levels. Hg° and O_3 mixing ratios decreased gradually, while Br_2 and aerosol Br^- increased slightly from outside to inside the 34 km MDE region. Variations in light alkanes and C_2H_2 exhibited the same patterns as those in Hg° and O_3. Air masses inside and outside the MDE were sampled at similar altitudes, and the air masses outside the MDE appeared to be transported along the same route as those inside the MDE. Thus, differences in mixing ratios of all trace gases were not as large as that in case 1.

In case 3, the MDE was sampled over a horizontal distance of ~143 km off the coast of northern Alaska. Ozone and Hg° mixing ratios declined steadily, Br_2 varied from 0.2 to 3.2 pptv, and water-soluble bromide was increased up to 19 pptv. Mixing ratios of BrO were ~4 pptv and decreased outside the MDE. Light alkanes and C_2H_2 tracked Hg° and O_3 well. Backward trajectories indicated that air masses traveled near the surface over the northern coast of Alaska and the Beaufort Sea from the Arctic Ocean. Air masses outside the MDE originated from the mid-troposphere. A spike of NO_x levels was observed in this case, which indicated fresh emissions likely coming from the oil refinery at Prudhoe Bay. The concurrent Hg° mixing ratio was 39 ppqv, possibly reflecting source emissions from the same area.

In case 4, the MDE area spanned 119 km over the Beaufort Sea and the Chukchi

ACPD
10, 10077–10112, 2010

Sea. Elemental mercury and O_3 decreased quickly from outside to inside the MDE. Water-soluble bromide varied from 12–19 pptv, and Br_2 increased quickly up to 5.5 pptv inside the MDE. The mixing ratio of BrO rose up to 8 pptv followed by a decline outside the MDE. Light alkanes and C_2H_2 followed the same trend in Hg° and O_3. Air masses inside the MDE appeared to be transported near the surface from northern Nunavut, whereas air masses outside the MDE were transported from Europe, Alaska, and the Northwest Territories in the mid–troposphere across the Arctic Ocean.

In cases 5, 6, and 7, mercury depletions spanned horizontal distances of 17, 68, and 56 km respectively, and were observed in the middle of the Arctic Ocean with similar transport pathways and origins of air masses primarily close to surface over the Arctic Ocean. All three cases showed declines in O_3, Hg°, and light alkanes with concomitant increases in Br_2, BrO, and water-soluble bromide.

Case 8 with a ~150 km L-shaped MDE area appeared to be more complicated than all other cases. Hg° mixing ratios exhibited a steep drop from 140 ppqv to the LOD upon entering the MDE area. However, O_3 levels hovered around 30-40 ppbv for the latter part of the MDE sampling, comparable to the levels outside the MDE. Moreover, this MDE was not accompanied by high levels of Br_2, BrO and water-soluble bromide. Air masses inside the MDE have two main origins, the Arctic Ocean and eastern Russia. Air masses outside the MDE were transported at mid- to upper-tropospheric altitudes from the northwestern Pacific and Russia. Very fresh combustion emissions were observed over the first 36 km of the MDE as indicated by enhanced mixing ratios of NO_x, Hg°, butane, and pentane. Backward trajectories suggested that the air masses came from the northern Alaska where high NO_x emissions comparable to the Prudhoe Bay Oil field were indicated by the 2002 EPA NO_x emissions map. Another unique feature in this case was that light alkanes and C_2H_2 tracked O_3 closely, but not Hg°.

ACPD
10, 10077–10112, 2010

4 Box model simulations

4.1 Base case results

The results of the base case are presented in Figures 4, 5, 6, and 7 and Table 4. We defined depletion as mixing ratios <50 ppqv for Hg° (~1.35×10^{6} molecules cm^{-3} at 255 K and 0.94 atm), 10 ppbv for O_3 (~2.71×10^{11} molecules cm^{-3}), and 25 pptv for C_2H_2 (~6.76×10^{8} molecules cm^{-3}). In the model runs Hg° was depleted in ~22 h, and about 97% of Hg° was transformed to up to 70 ppqv $HgBr_2$. HgO was the second most abundant RGM species, but its level was about 45-fold less than that of $HgBr_2$. Some studies assumed a radical reaction such as the HgBr + BrO reaction in the Arctic spring (Calvert and Lindberg, 2003; Xie et al., 2008), and BrHgOBr was one of the main RGM products. This radical reaction was not included in our model due to a lack of experimental rate constants. Ozone was depleted in 23 h, and C_2H_2 was depleted in ~36 h. Ethyne decreased very rapidly due to the reaction with abundant Br radical after O_3 was reduced to <1 ppbv. Cases 1–6 of the ARCTAS measurements showed comparatively distinct declines of C_2H_2 and light alkanes compared to the simulation results. Ethyne was not depleted in the field observations, but the range of decrement was significant spanning 72–420 pptv from outside to inside the MDEs. In the simulations C_2H_2 was decreased by 340 pptv, which was in the same range as the observations. Light alkanes were also consistently decreased during the 100 h of simulation. For example, C_2H_6 decreased to ~32% of its initial concentration and C_4H_{10} declined to about 76% of its initial concentration after 100 h of simulation. A decline of 205–920 pptv in ethane was observed from outside to inside the MDEs compared to about a decrease of ~600 pptv after 100 h of simulation. Thus, our box model simulations appear to be able to reproduce the decreases of various light alkanes and C_2H_2 captured in the ARCTAS measurements as well as depletion of Hg° and O_3. This suggests that the chemistry represented in the box model sufficiently depicts chemical processes conducive to the occurrence of MDEs and O_3 depletion events (ODEs).

ACPD
10, 10077–10112, 2010

Furthermore, we simulated conditions without O_3 chemistry but included O_3 photolysis in our chemical mechanism. It indicated that certain levels of O_3 provided an additional sink of halogen radicals including Br, and hence the time to reach Hg° depletion was longer. The results suggest a close relation between O_3 and Hg°, and thus we conducted simulations with O_3 chemistry afterwards to make them more realistic.

4.2 Influence of rate constant values

Applying different rate constants for Hg° reactions with Cl, OH, and Br_2 did not affect the time it took to reach depletion (denoted as τ_{dep}) of Hg° (Table A in the supplementary document http://www.atmos-chem-phys-discuss.net/10/10077/2010/acpd-10-10077-2010-supplement.pdf and Fig. 4). However, different rate constants for Hg° reaction with Br influenced the final product composition and τ_{dep}. The amounts of HgO, $HgCl_2$, and $Hg(OH)_2$ produced were the greatest using the Donohoue et al. (2006) rate constant value compared to application of other values. Using the rate constants of Donohoue et al. (2006) and Khalizov et al. (2003) led to a slow decrease in Hg° at first followed by a faster decline compared to the base case. Furthermore, the variation in the rate constant values of Hg° reaction with Br was also important in determining τ_{dep}. Compared to the base case, using the rate constant from Khalizov et al. (2003) and Donohoue et al. (2006) increased τ_{dep} (Table 4). However, about 97% of the RGM product was $HgBr_2$, the same as in the base run case.

The rate constant of Hg° with BrO varies over the range of 1×10^{-15}–1×10^{-13} cm^3 $molecule^{-1}$ s^{-1} at 298 K (Raofie and Ariya, 2003) and the temperature dependent rate constants were not provided in that study. We ran three simulations using rate constants of 1×10^{-13}, 1×10^{-14}, and 1×10^{-15} cm^3 $molecule^{-1}$ s^{-1} in base case run to study the influence of the reaction on Hg° depletion. With the slowest rate constant, Hg° reaction with BrO was negligible. With the fastest rate constant, the τ_{dep} value for Hg° was reduced by 8 h and slightly more HgO was produced than $HgBr_2$. When the temperature of 255 K was considered, the reaction of Hg° with BrO did not seem to be important in our simulations, which suggests negligible effect of Hg°

ACPD
10, 10077–10112, 2010

reaction with BrO on the occurrence of MDEs in the Arctic spring.

4.3 Influence of halogen radical concentrations

A simulation was conducted without halogen compounds being re-set to the initial conditions at each time step. It was found that ~11% of Hg° was transformed to RGM and O_3 was decreased by ~0.5% after 100 h of simulation. This suggested that continuous emission of halogen compounds is imperative to the occurrence of MDEs and ODEs in the Arctic springtime.

In addition, simulations were performed using 3 and 5 pptv Br_2 and 5 pptv Cl_2 (Fig. 5 and Table 4). We found that the higher the Br_2 concentration was, the faster the Hg°, O_3, and C_2H_2 depletion occurred. The τ_{dep} value decreased almost linearly with increases in Br_2. Adding 5 pptv of Cl_2 reduced the τ_{dep} value for each compound by 20–30 min. The rate constant of Cl and Br with Hg° are of same order of magnitude, 10^{-12} cm^3 $molecule^{-1}$ s^{-1} at 255 K. However, the order of magnitude for the rate constant of Cl radical with hydrocarbons and O_3 are 10^{-11} cm^3 $molecule^{-1}$ s^{-1} except n-C_4H_{10}, 10^{-10} cm^3 $molecule^{-1}$ s^{-1}; the reactivity of Br radical with O_3 is 10^{-13} cm^3 $molecule^{-1}$ s^{-1} and that of Br radical with C_2H_2 is 10^{-14} cm^3 $molecule^{-1}$ s^{-1}. Furthermore, there was a lack of bromine reactions with light alkanes in the model due to insufficient kinetic information available in literature. Therefore, the high reactivity of Cl with abundant hydrocarbons and O_3 caused τ_{dep} value for Hg° to be much more sensitive to Br_2 than Cl_2. Approximately 99% of the RGM product was $HgBr_2$, with the higher Br_2 cases showing a slight increase in the amount of $HgBr_2$. ARCTAS measurement data showed that Br_2 mixing ratios varied over 1–7 pptv in most MDEs, and thus it is reasonable to speculate based on our box model simulations that Br_2 (Br) played an important role in the occurrence of MDEs.

At the 5 pptv Cl_2 mixing ratios of light alkanes decreased significantly compared to cases with additional input of Br_2. For instance, we found a 70% decrease in C_2H_6 in 100 h for 5 pptv Cl_2 compared to a ~35% decrease in other cases.

ACPD
10, 10077–10112, 2010

4.4 Influence of photolysis rate constants

Different photolysis rate constants affected the τ_{dep} value for Hg° (Table 3 and 4 and Fig. 6) and higher photolysis rate constants drove faster depletion for Hg°. The main RGM product was again $HgBr_2$. However, HgO, the second most abundant RGM product in the high photolysis case was about 52% of its values in the base case because fast production of Br radicals accelerated the $Hg^{\circ} + Br$ reaction. Moreover, the higher photolysis case showed a more rapid decrease in C_2H_2 and O_3 compared to the lower photolysis. Light alkanes also showed faster decreases in the high photolysis case and slower decreases in the low photolysis case (e.g., C_2H_6 showed a 62 % decrease in the high photolysis case and a 21% decrease in the low photolysis case after 100 h of simulation). We examined the ARCTAS measurements for correlation between the Br_2 photolysis rate constant and O_3 mixing ratios inside the MDE regions, but we did not find a strong relationship. This is probably not surprising since the depletion events were sampled at various stages of their lifetime.

4.5 High versus low NO_x regimes

ARCTAS measurements showed that the NO mixing ratio was commonly about 10 pptv and NO_2 was ~0 pptv. However, a couple of cases showed very high mixing ratios of NO and NO_2 for short time periods which indicated an influence of fresh emissions from northern Alaska, including the Prudhoe Bay Oil field. This motivated simulations of high and low NO_x regimes.

The low NO_x regime was based on case 7 of the eight ARCTAS MDEs. The results for low NO_x were similar to the base case (Fig. 7). In the high NO_x regime, Cl radical concentration was slightly increased during the 100 h of simulation due to acceleration of Cl production from the reaction of ClO + NO. Thus light alkanes decreased slightly more than in the base case after 100 h of simulation due to reaction of light alkanes with the Cl radical.

Different from Cl, Br reactions with light alkanes were not implemented in our model,

ACPD
10, 10077–10112, 2010

and thus high NO_x concentrations significantly increased the Br radical concentration in comparison to the Cl radical. Fast production of Br radicals in the high NO_x regime occurred during the first part (33 h) of simulation, with a decreased BrO amount. Increased Br radical concentrations were presumably due to the reaction of BrO with NO. Thus, O_3 and Hg° depletion occurred ~2 h for O_3 and ~16 h for Hg° sooner compared to the base case (Table 4). Ethyne declined at a faster rate initially in the high NO_x regime compared to the base case because of its reaction with Br radical, but overall the depletion time in the high NO_x regime was similar to that of the base case. Note that these results suggested that the impact of high NO_x regime on Hg° depletion could be exaggerated slightly due to the lack of rate constants of Br with light alkanes.

Moreover, we simulated the corresponding chemical environments at higher NO_x levels based on ARCTAS measurements. This simulation showed that higher-NO_x induced changes in hydrocarbon concentrations slightly affected the RGM composition and τ_{dep} for Hg° in high NO_x regime. Compared to the high NO_x level alone, τ_{dep} for Hg° was prolonged by 30 min, and HgO production was increased by 11%. The τ_{dep} value for O_3 was prolonged by 1.5 h.

We did not find distinguishable characteristics for O_3, C_2H_2, and light alkanes in the high NO_x regimes from the ARCTAS measurements, but Hg° was 28–44 ppqv during these time periods in cases 3 and 8 with a possible contribution from combustion. However, these levels were still low compared to the values outside the MDEs, and indicated the possibility of fast Hg° oxidation in the high NO_x regime as shown in model simulations.

5 Conclusions

Atmospheric MDEs observed during the ARCTAS field campaign were investigated by analysis of aircraft data and box modeling. MDEs were observed to occur near the surface over the Arctic Ocean with coincident O_3 depletion, high Br_2 levels, and decreases in light alkanes and C_2H_2. Generally, air masses inside the MDEs transported at low

levels over the ocean, and thus a distinguishable chemical feature of the air is that it is likely halogen rich.

We developed a gas phase box model including mercury, halogen species, and ozone chemistry with input from the ARCTAS measurements. We simulated several sensitivity experiments to study the influence of variable rate constants of Hg° chemistry, concentrations of halogen compounds, photolysis rate constant values, and NO_x mixing ratios on Hg° depletion. The results suggested that high Br_2 mixing ratios, high photolysis rate constants, and high NO_x regime caused accelerated Hg° depletion. These three environments accelerated Br radical production and hence increased the rate of Hg° depletion. Moreover, we found that Hg° responded in a more sensitive manner to the variations in the chemical environment compared to O_3. This could possibly explain the moderate decreases in O_3 mixing ratios in MDE regions compared to total depletion of Hg°.

Finally, thinking about how climate change in the Arctic might affect MDEs produced the following possible scenarios. Climate change has driven a decreasing amount of ice surface area over the Arctic Ocean, and thus should promote increasing amounts of halogen compounds released into boundary layer air. This implies the possibility of more frequent and widespread occurrence of springtime MDEs. On the other hand, a larger open ocean would foster more turbulence in the atmosphere above, and perhaps cause reduced occurrence of pronounced MDEs. Since the ocean is a large natural source of Hg° (Selin, 2009; Sigler et al., 2009), this might also serve to reduce MDEs. It will be interesting to observe in the future the impact of reduced Arctic pack ice on chemical cycling of trace gases like Hg° that are sensitive to such processes.

Acknowledgements. This research benefited considerably from the combined effort of NASA DC-8 flight and science teams for ARCTAS. We are grateful to NASA Earth Science Tropospheric Chemistry Program for ARCTAS funding which supported this work. Funding for this work was also provided by the NOAA AIRMAP grant #NA06OAR4600189. We also thank Mikhail Zhukovskiy, Che-Jen Lin and Oliver W. Wingenter for useful input during our box model development. We thank Barkley Sive and Howard Mayne for helpful discussions.

References

Ariya, P. A., Khalizov, A., and Gidas, A.: Reactions of Gaseous Mercury with Atomic and Molecular Halogens: Kinetics, Product Studies, and Atmospheric Implications, J. Phys. Chem. A, 106, 7310–7320, 2002.

Ariya, P. A., Dastoor, A. P., Amyot, M., Schroeder, W. H., Barrie, L., Anlauf, K., Raofie, F., Ryzhkov, A., Davignon, D., Lalonde, J., and Steffen, A.: The Arctic: a sink for mercury, Tellus, 56B, 397–403, 2004.

Atkinson, R., Baulch, D. L., Cox, R. A., Crowley, J. N., Hampson, R. F., Hynes, R. G., Jenkin, M. E., Rossi, M. J., and Troe, J.: Evaluated kinetic and photochemical data for atmospheric chemistry: Volume I – gas phase reactions of O_x, HO_x, NO_x, and SO_x species, Atmos. Chem. Phys., 4, 1461–1738, 2004, http://www.atmos-chem-phys.net/4/1461/2004/.

Atkinson, R., Baulch, D. L., Cox, R. A., Crowley, J. N., Hampson, R. F., Hynes, R. G., Jenkin, M. E., Rossi, M. J., and Troe, J.: Evaluated kinetic and photochemical data for atmospheric chemistry: Volume II – gas phase reactions of organic species, Atmos. Chem. Phys., 6, 3625–4055, 2006, http://www.atmos-chem-phys.net/6/3625/2006/.

Atkinson, R., Baulch, D. L., Cox, R. A., Crowley, J. N., Hampson, R. F., Hynes, R. G., Jenkin, M. E., Rossi, M. J., and Troe, J.: Evaluated kinetic and photochemical data for atmospheric chemistry: Volume III – gas phase reactions of inorganic halogens, Atmos. Chem. Phys., 7, 981–1191, 2007, http://www.atmos-chem-phys.net/7/981/2007/.

Balabanov, N. B., Shepler, B. C., and Peterson, K. A.: Accurate Global Potential Energy Surface and Reaction Dynamics for the Ground State of $HgBr_2$, J. Phys. Chem. A, 109, 8765–8773, 2005.

Branfireun, B. A., Krabbenhoft, D. P., Hintelmann, H., Hunt, R. J., Hurley, J. P., and Rudd, J. W. M.: Speciation and transport of newly deposited mercury in a boreal forest wetland: A stable mercury isotope approach, Water Resour. Res., 41, W06016, doi:10.1029/2004WR003219, 2005.

Calvert, J. G. and Lindberg, S. E.: A modeling study of the mechanism of the halogen-ozone-mercury homogeneous reactions in the troposphere during the polar spring, Atmos. Environ., 37, 4467–4481, 2003.

Cobbett, F. D., Steffen, A., Lawson, G., and Van Heyst, B. J.: GEM fluxes and atmospheric mercury concentrations (GEM, RGM, and Hg^p) in the Canadian Arctic at Alert, Nunavut, Canada (February–June 2005), Atmos. Environ., 41, 6527–6543, 2007.

Colman, J. J., Swanson, A. L., Meinardi, S., Sive, B. C., Blake, D. R., and Rowland, F. S.: Description of the analysis of a wide range of volatile organic compounds in whole air samples collected during PEM-Tropics A and B, Anal. Chem., 73, 3723–3731, 2001.

Dibb, J. E., Talbot, R. W., Scheuer, E. M., Seid, G., Avery, M. A., and Singh, H. B.: Aerosol chemical composition in Asian continental outflow during the TRACE-P campaign: Comparison with PEM-West B, J. Geophys. Res., 108, 8815, doi:10.1029/2002JD003111, 2003.

Donohoue, D. L., Bauer, D., and Hynes, A. J.: Temperature and Pressure Dependant Rate Coefficients for the Reaction of Hg with Cl and the Reaction of Cl with Cl: A Pulsed Laser Photolysis-Pulsed Laser Induced Fluorescence Study, J. Phys. Chem. A, 109(34), 7732–7741, 2005.

Donohoue, D. L., Bauer, D., Cossairt, B., and Hynes, A. J.: Temperature and Pressure Dependant Rate Coefficients for the Reaction of Hg with Br and the Reaction of Br with Br: A Pulsed Laser Photolysis-Pulsed Laser Induced Fluorescence Study, J. Phys. Chem. A, 110(21), 6623–6632, 2006.

Eneroth, K., Holmén, K., Berg, T., Schmidbauer, N., and Solberg, S.: Springtime depletion of tropospheric ozone, gaseous elemental mercury and non-methane hydrocarbons in the European Arctic, and its relation to atmospheric transport, Atmos. Environ., 41, 8511–8526, 2007.

Fain, X., Ferrari, C. P., Gauchard, P.-A., Magand, O., and Boutron, C.: Fast depletion of gaseous elemental mercury in the Kongsvegen Glacier snowpack in Svalbard, Geophys. Res. Lett., 33, L06826, doi:10.1029/2005GL025223, 2006.

Fuelberg, H., Loring, Jr., R., Watson, M., Sinha, M., Pickering, K., Thompson, A., Sachse, G., Blake, D., and Schoeber, M.: TRACE-A trajectory intercomparison 2. Isentropic and kinematic methods, J. Geophys. Res., 101, 23927–23939, 1996.

Fuelberg, H. E., Hannan, J. R., van Velthoven, P. F. J., Browell, E. V., Bieberbach, Jr., G., Knabb, R. D., Gregory, G. L., Pickering, K. E., and Selkirk, H. B.: A meteorological overview of the Subsonic Assessment Ozone and Nitrogen Oxide Experiment (SONEX) period, J. Geophys. Res., 105, 3633–3651, 2000.

Goodsite, M. E., Plane, J. M. C., and Skov, H.: A Theoretical Study of the Oxidation of Hg^0 to $HgBr_2$ in the Troposphere, Environ. Sci. Technol., 38, 1772–1776, 2004.

Hall, B.: The Gas Phase Oxidation of Elemental Mercury by Ozone, Water, Air Soil Poll., 80, 301–315, 1995.

Hedgecock, I. M., Trunfio, G. A., Pirrone, N., and Sprovieri, F.: Mercury chemistry in the MBL:

Mediterranean case and sensitivity studies using the AMCOTS (Atmospheric Mercury Chemistry over the Sea) model, Atmos. Environ., 39, 7217–7230, 2005.
Khalizov, A. F., Viswanathan, B., Larregaray, P., and Ariya, P. A.: A Theoretical Study on the Reactions of Hg with Halogens: Atmospheric Implications, J. Phys. Chem. A, 107, 6360–6365, 2003.
Lehrer, E., Hönninger, G., and Platt, U.: A one dimensional model study of the mechanism of halogen liberation and vertical transport in the polar troposphere, Atmos. Chem. Phys., 4, 2427–2440, 2004, http://www.atmos-chem-phys.net/4/2427/2004/.
Lin, C.-J. and Pehkonen, S. O.: The chemistry of atmospheric mercury: a review, Atmos. Environ., 33, 2067–2079, 1999.
Lindberg, S. E., Brooks, S., Lin, C.-J., Scott, K. J., Landis, M. S., Stevens, R. K., Goodsite, M., and Richter, A.: Dynamic Oxidation of Gaseous Mercury in the Arctic Troposphere at Polar Sunrise, Environ. Sci. Technol., 36, 1245–1256, 2002.
Lu, J. Y., Schroeder, W. H., Barrie, L. A., Steffen, A., Welch, H. E., Martin, K., Lockhart, L., Hunt, R. V., Boila, G., and Richter, A.: Magnification of atmospheric mercury deposition to polar regions in springtime: the link to tropospheric ozone depletion chemistry, Geophys. Res., Lett., 28(17), 3219–3222, 2001.
Magarelli, G., and Fostire, A. H.: Influence of deforestation on the mercury air/soil exchange in the Negro River Basin, Amazon, Atmos. Environ., 39, 7518-7528, 2005.
Malcolm, E. G., Keeler, G. J., and Landis, M. S.: The effects of the coastal environment on the atmospheric mercury cycle, J. Geophys. Res., 108(D12), 4357, doi:10.1029/2002JD003084, 2003.
Mao, H., Talbot, R., Sive, B., Kim, S. Y., Blake, D. R., and Weinheimer, A. J., Arctic mercury depletion and its quantitative link with halogens, J. Geophys. Res., submitted, 2010.
Martin, B. D., Fuelberg, H. E., Blake, N. J., Crawford, J. H., Logan, J. A., Blake, D. R., and Sachse, G. W.: Long range transport of Asian outflow to the equatorial Pacific, J. Geophys. Res., 108(D2), 8322, doi:10.1029/2001JD001418, 2003.
Neuman, J. A., Nowak, J. B., Huey, L. G., Burkholder, J. B., Dibb, J. E., Holloway, J. S., Liao, J., Peischl, J., Roberts, J. M., Ryerson, T. B., Scheuer, E., Stark, H., Stickel, R. E., Tanner, D. J., and Weinheimer, A.: Bromine measurements in ozone depleted air over the Arctic Ocean, Atmos. Chem. Phys. Discuss., 10, 3827–3860, 2010, http://www.atmos-chem-phys-discuss.net/10/3827/2010/.
Pal, B. and Ariya, P. A.: Gas-Phase HO-Initiated Reactions of Elemental Mercury: Kinet-

ics, Product Studies, and Atmospheric Implications, Environ. Sci. Technol., 38, 5555–5566, 2004a.
Pal. B. and Ariya, P. A.: Studies of ozone initiated reactions of gaseous mercury: kinetics, product studies, and atmospheric implications, Phys. Chem. Chem. Phys., 6, 572–579, 2004b.
Pan, L. and Carmichael, G. R.: A Two-Phase Box Model to Study Mercury Atmospheric Mechanism, Environ. Chem., 2, 205-214, 2005.
Poissant, L., Pilote, M., Beauvais, C., Constant, P., and Zhang, H. H.: A year of continuous measurements of three atmospheric mercury species (GEM, RGM, and Hg_p) in southern Québec, Canada, Atmos. Environ., 39, 1275-1287, 2005.
Raofie, F. and Ariya, P. A.: Kinetics and products study of the reaction of BrO radicals with gaseous mercury, J. Phys. IV France, 107, 1119–1121, 2003.
Ridley, B. A., Grahek, F. E., and Walega, J. G.: A small high-sensitivity, medium- response ozone detector suitable for measurements from light aircraft, J. Atmos. Oceanic Technol., 9, 142–148, 1992.
Saiz-Lopez, A., Saunders, R. W., Joseph, D. M., Ashworth, S. H., and Plane, J. M. C.: Absolute absorption cross-section and photolysis rate of I_2, Atmos. Chem. Phys., 4, 1443–1450, 2004, http://www.atmos-chem-phys.net/4/1443/2004/.
Sander, S. P., Finlayson-Pitts, B. J., Friedl, R. R., Golden, D. M., Huie, R. E., Kolb, C. E., Kurylo, M. J., Molina, M. J., Moortgat, G. K., Wine, P. H., Keller-Rudek, H., Orkin, V. L., and Ravishankara, A. R.: Chemical Kinetics and Photochemical Data for Use in Atmospheric Studies, Evaluation Number 15, JPL Publication 06-2, Jet Propulsion Laboratory, Pasadena, CA, USA, 2006.
Sandu, A. and Sander, R.: Technical note: Simulating chemical systems in Fortran90 and Metlab with the Kinetic PreProcessor KPP-2.1, Atmos. Chem. Phys., 6, 187–195, 2006, http://www.atmos-chem-phys.net/6/187/2006/.
Scheuer, E., Talbot, R. W., Dibb, J. E., Seid, G. K., DeBell, L., and Lefer, B.: Seasonal distributions of fine aerosol sulfate in the North American Arctic basin during TOPSE, J. Geophys. Res., 108, 8370, doi:10.1029/2001JD001364, 2003.
Schroeder, W. H. and Munthe, J.: Atmospheric Mercury-An Overview, Atmos. Environ., 32, 809–822, 1998.
Schroeder, W. H., Anlauf, K. G., Barrie, L. A., Lu, J. Y., Steffen, A., Schneeberger, D. R., and Berg, T. : Arctic springtime depletion of mercury, Nature, 394, 331–332, 1998.
Selin, N. E.: Global Biogeochemical Cycling of Mercury: A Review, Annu. Rev. Environ. Re-

sour., 34, 43–63, 2009.
Sigler, J. M., Mao, H., Sive, B. C., and Talbot, R.: Oceanic influence on atmospheric mercury at coastal and inland sites: a springtime noreaster in New England, Atmos. Chem. Phys., 9, 4023–4030, 2009, http://www.atmos-chem-phys.net/9/4023/2009/.
Simpson, W. R., von Glasow, R., Riedel, K., Anderson, P., Ariya, P., Bottenheim, J., Burrows, J., Carpenter, L. J., Frieβ, U., Goodsite, M. E., Heard, D., Hutterli, M., Jacobi, H.-W., Kaleschke. L., Neff, B., Plane, J., Platt, U., Richter, A., Roscoe, H., Sander, R., Shepson, P., Sodeau, J., Steffen, A., Wagner, T., and Wolff, E.: Halogens and their role in polar boundary-layer ozone depletion, Atmos. Chem. Phys., 7, 4375–4418, 2007, http://www.atmos-chem-phys.net/7/4375/2007/.
Sommar, J., Gårdfeldt, K., Strömberg, D., and Feng, X., A kinetic study of the gas-phase reaction between the hydroxyl radical and atomic mercury, Atmos. Environ., 35, 3049–3054, 2001.
Strode, S. A., Jaeglé, L., Selin, N. E., Jacob, D. J., Park, R. J., Yantosca, R. M., Mason, R. P., and Slemr, F.: Air-sea exchange in the global mercury cycle, Global Biogeochem. Cycles, 21, GB1017, doi:10.1029/2006GB002766, 2007.
Talbot, R., Mao, H., Scheuer, E., Dibb, J., Avery, M., Browell, E., Sachse, G., Vay, S., Blake, D., Huey, G., and Fuelberg, H.: Factors influencing the large-scale distribution of Hg° in the Mexico City area and over the north Pacific, Atmos. Chem. Phys., 8, 2103–2114, 2008, http://www.atmos-chem-phys.net/8/2103/2008/.
Tokos, J. J. S., Hall, B., Calhoun, J. A., and Prestbo, E. M.: Homogeneous gas-phase reaction of Hg° with H_2O_2, O_3, CH_3I, and $(CH_3)_2S$: implications for atmospheric Hg cycling, Atmos. Environ., 32, 823–827, 1998.
Verwer, J., Spee, E., Blom, J. G., and Hunsdorfer, W.: A second order Rosenbrock method applied to photochemical dispersion problems, SIAM Journal on Scientific Computing, 20, 1456–1480, 1999.
Xie, Z.-Q., Sander, R., Pöschl, U., and Slemr, F.: Simulation of atmospheric mercury depletion events (AMDEs) during polar springtime using the MECCA box model, Atmos. Chem. Phys., 8, 7165–7180, 2008, http://www.atmos-chem-phys.net/8/7165/2008/.

Table 1. MDE cases selected for study.

case	day	Universal Time (s)	O_3 (ppbv)	Hg° (ppqv)	Br_2 (pptv)
				(below detection level except several points mentioned below)	
1	8/4/2008	62 520–64 200	0.38–5.6	one–22	3.25–5.8
2	9/4/2008	64 320–64 560	5.0–13.5	two–21	1.3–2.7
3	16/4/2008	75 720–76 740	1.8–34.5	one–39	0.2–3.2
4	16/4/2008	79 980–80 820	3.3–43	25, 34, and 37	0.45–5.4
5	17/4/2008	83 160–83 280	0.8–30		1.5–6.15
6	17/4/2008	88 140–88 680	10.7–34.5	24, and 62	1.05–6.85
7	17/4/2008	97 380–97 800	9.0–26.5		0.75–2.75
8	17/4/2008	101 220–102 900	0.9–42	28–61	0.35–1.75

Table 2. Initial conditions used in model runs.

Chemical compounds	Mixing ratios/concentrations
NO	10 pptv
NO_2	0 pptv
H_2O_2	152 pptv
HCHO	122 pptv
OH	360 000 #/cm^3
CH_3OH	608 pptv
CH_3CHO	121 pptv
C_2H_6	1873 pptv
C_2H_2	364 pptv
C_3H_8	542 pptv
n-C_4H_{10}	111 pptv
CH_4	1880 ppbv
C_2H_5OH	63 pptv
HO_2	2.72 pptv
CH_3Br	9.2 pptv
O_3	35 ppbv
Hg°	122 ppqv
I_2	1 pptv
Br_2	1 pptv
Cl_2	2 pptv
CO	159 ppbv
H_2O	1203 ppmv

Table 3. Photolysis rate constants (unit: s^{-1}).

	middle	high	low
$Br_2 \rightarrow Br + Br$	0.029	0.049	0.015
$BrO \rightarrow Br + O$	0.020	0.043	0.014
$HOBr \rightarrow HO + Br$	0.0015	0.0029	0.00092
$BrCl \rightarrow Br + Cl$	0.0083	0.015	0.0048
$BrONO_2 \rightarrow Br + NO_3$	0.00014	0.00026	8.33×10^{-5}
$BrONO_2 \rightarrow BrO + NO_2$	0.00077	0.0015	0.00047
$Cl_2 \rightarrow Cl + Cl$	0.0013	0.0028	0.00089
$ClONO_2 \rightarrow Cl + NO_3$	1.91×10^{-5}	4.0×10^{-5}	1.26×10^{-5}
$ClONO_2 \rightarrow ClO + NO_2$	2.14×10^{-6}	5.29×10^{-6}	1.47×10^{-6}
$O_3 \rightarrow O_2 + O(^1D)$	1.89×10^{-6}	6.6×10^{-6}	1.22×10^{-6}
$NO_2 \rightarrow NO_2 + O$	0.0057	0.01	0.0036
$CH_3CHO \rightarrow CH_3 + CHO$	6.53×10^{-7}	2.1×10^{-6}	4.2×10^{-7}
$HCHO \rightarrow H + HCO$	9.2×10^{-6}	2.35×10^{-5}	6.2×10^{-6}
$HCHO \rightarrow H_2 + CO$	2.04×10^{-5}	4.65×10^{-5}	1.43×10^{-5}
$CH_3OOH \rightarrow CH_3O + OH$	2.03×10^{-6}	4.75×10^{-6}	1.4×10^{-6}
$N_2O_5 \rightarrow NO_2 + NO_3$	9.84×10^{-6}	2.4×10^{-5}	7.03×10^{-6}
$H_2O_2 \rightarrow 2\,OH$	2.18×10^{-6}	5.24×10^{-6}	1.5×10^{-6}

ACPD
10, 10077–10112, 2010

Table 4. Prominent τ_{dep} values for several sensitivity experiment results.

		τ_{dep} (h)		
		Hg°	O_3	C_2H_2
Base		21.9	23.1	35.9
Rate constant of Hg° + Br	Khalizov et al. (2003)	28.4	23.1	35.9
	Donohoue et al. (2006)	32	23.1	35.9
Different Br_2 mixing ratio	3 pptv	7.6	15.5	23.4
	5 pptv	3.4	9.3	14.2
Different photolysis constant	High	10	19.9	30.3
	Low	32.7	25.6	41.6
High NO_x regime		5.6	21.2	36.1

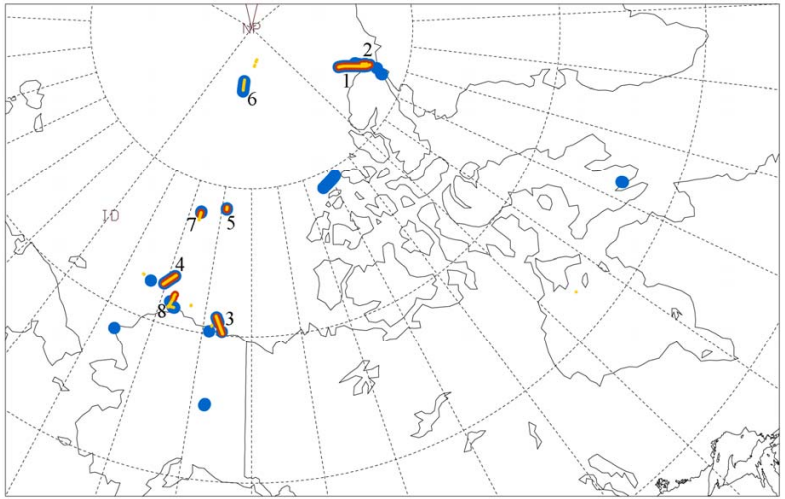

Fig. 1. Spatial distribution of Hg°<50 ppqv (yellow dots), O_3<10 ppbv (red dots), and high Br_2>2 pptv (blue dots) below 5 km altitude.

ACPD

10, 10077–10112, 2010

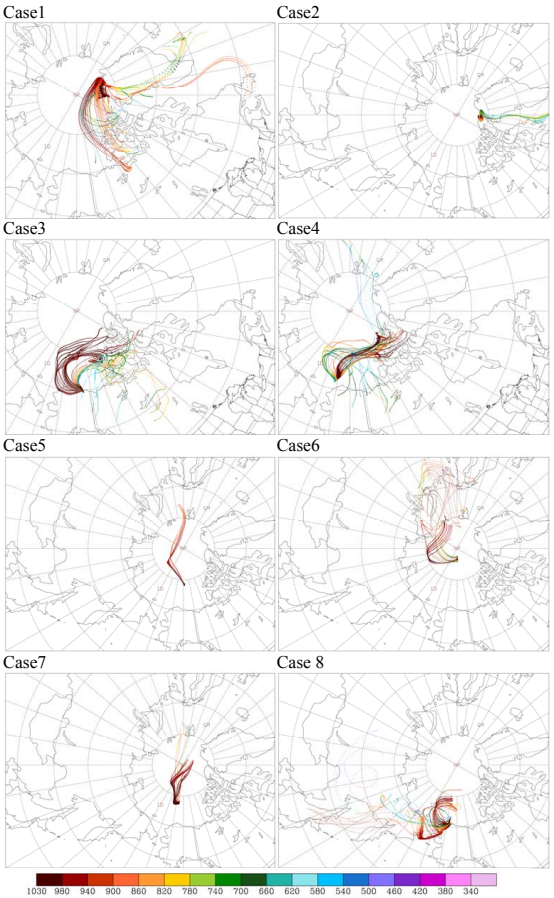

Fig. 2. Five-day backward trajectories for each MDE case.

ACPD
10, 10077–10112, 2010

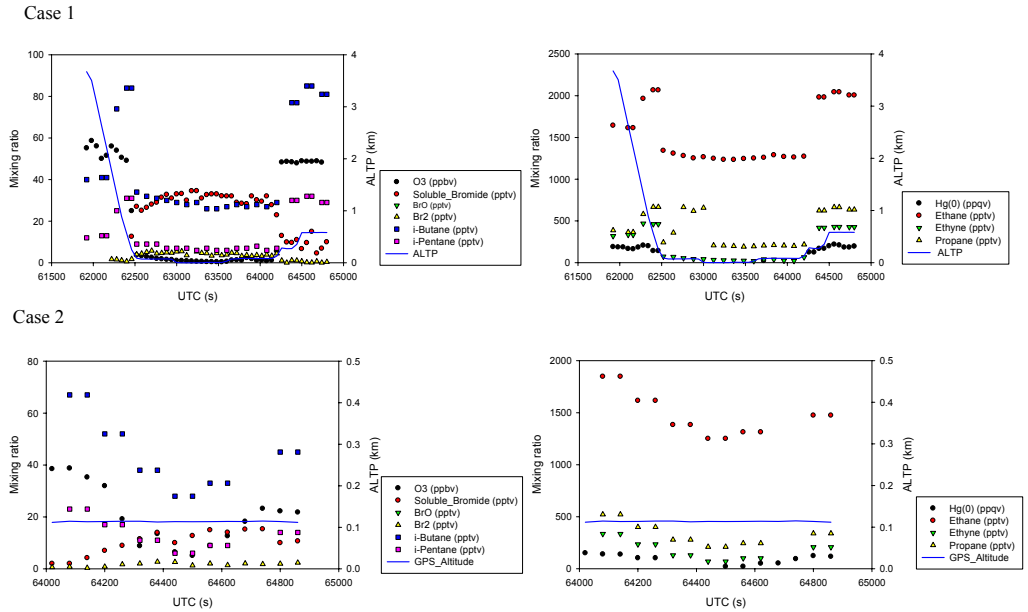

Fig. 3. Mixing ratios of Hg°, O_3, halogen compounds, and hydrocarbons for each MDE case. Units are ppbv for O_3, ppqv for Hg°, and pptv for other species.

ACPD
10, 10077–10112, 2010

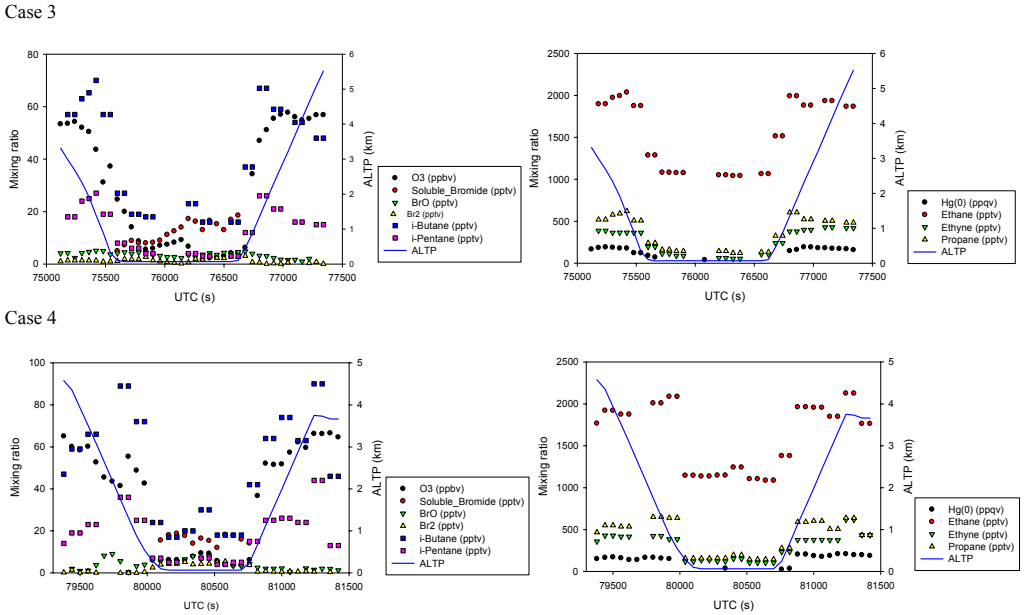

Fig. 3. Continued.

ACPD
10, 10077–10112, 2010

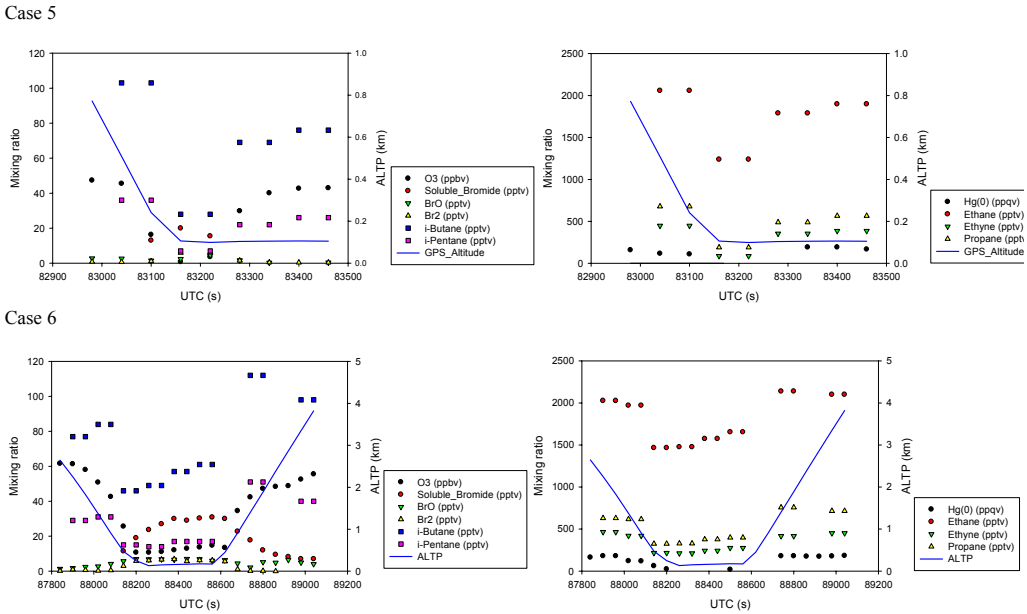

Fig. 3. Continued.

ACPD
10, 10077–10112, 2010

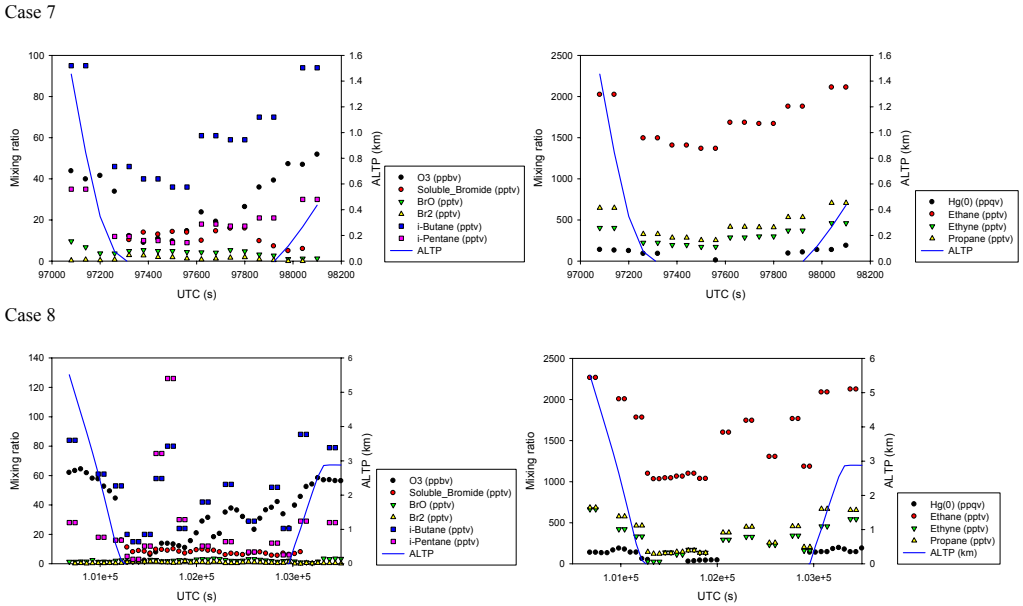

Fig. 3. Continued.

ACPD
10, 10077–10112, 2010

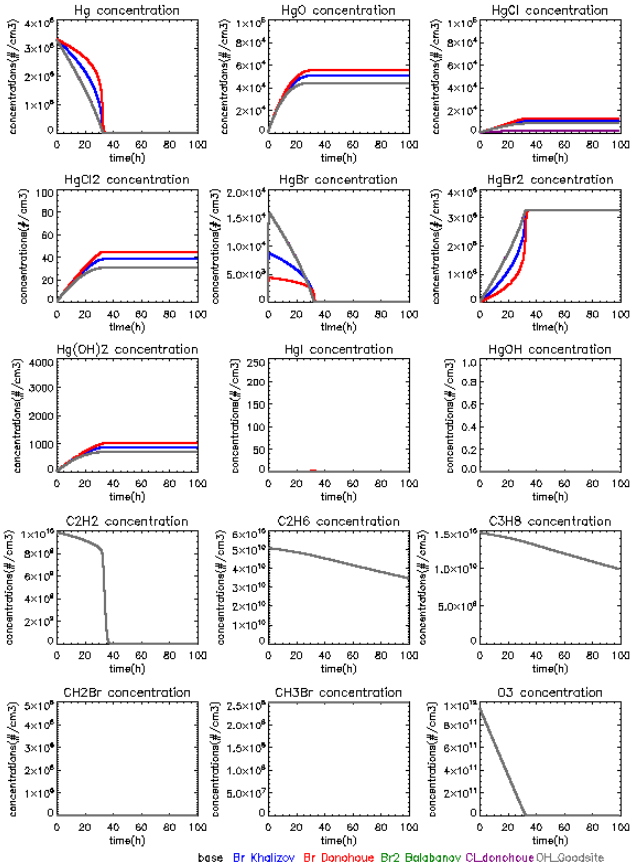

Fig. 4. 100 h model simulation for different rate constants. Black is base run, blue is Khalizov et al. (2003) and red is Donohoue et al. (2006) for $Hg^{\circ} + Br$, green is Balabanov et al. (2005) for $Hg^{\circ} + Br_2$, purple is Donohoue et al. (2005) for $Hg^{\circ} + Cl$, and grey is Goodsite et al. (2004) for $Hg^{\circ} + OH$.

ACPD
10, 10077–10112, 2010

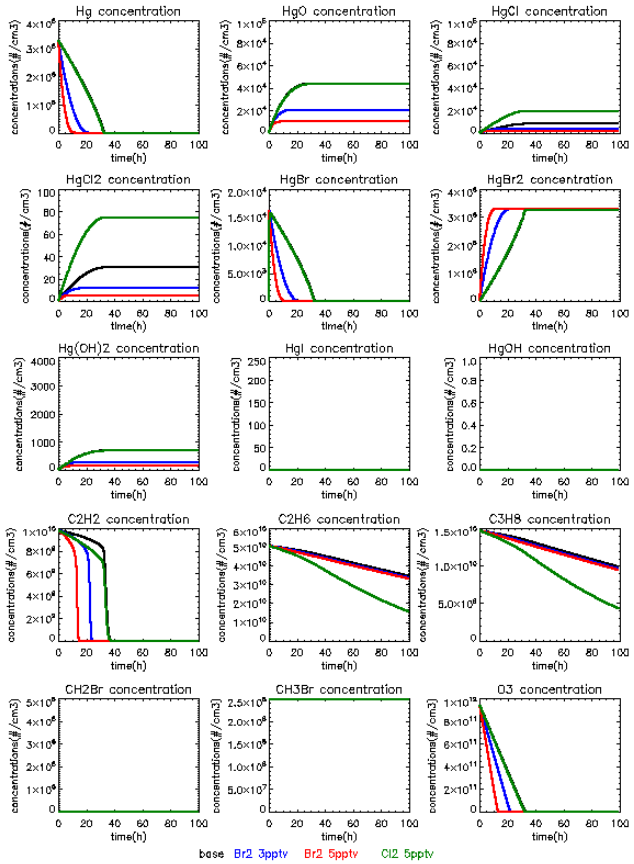

Fig. 5. 100 h model simulation using different halogen mixing ratios. Black is base run, blue is 3 pptv Br_2, red is 5 pptv Br_2, and green is 5 pptv Cl_2.

ACPD
10, 10077–10112, 2010

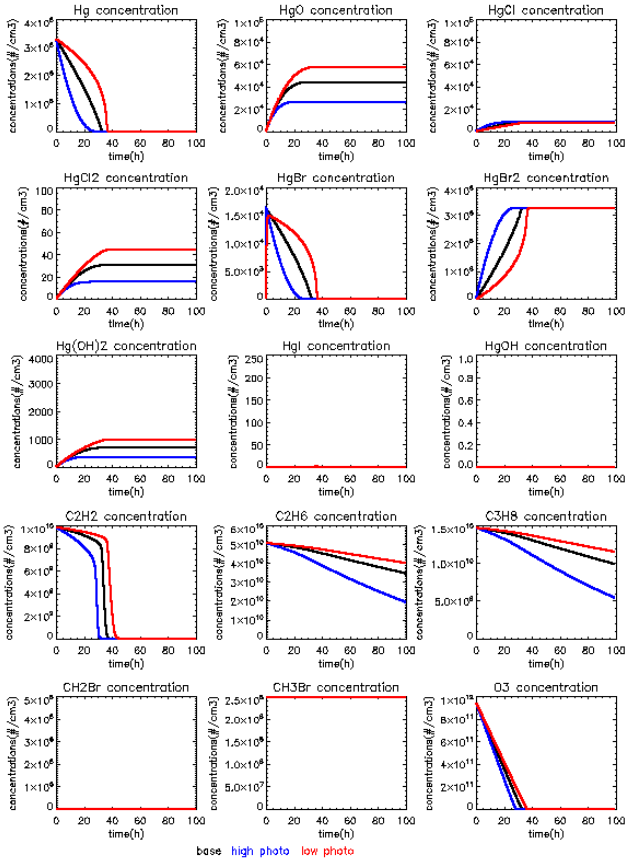

Fig. 6. 100 h model simulation for different photolysis rate constants. Black is base run, blue is high photolysis case, and red is low photolysis case.

ACPD
10, 10077–10112, 2010

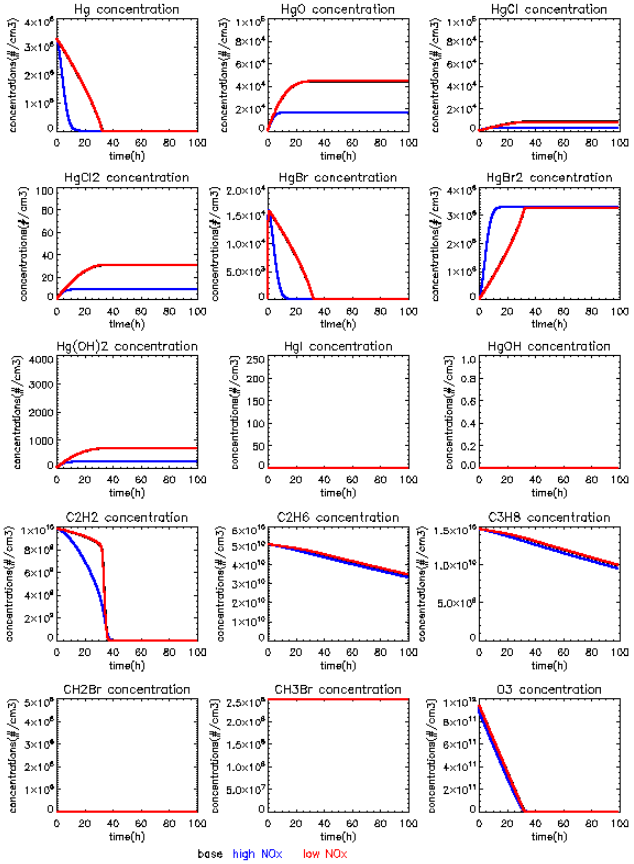

Fig. 7. 100 h model simulation for high NO_x and low NOx regime. Black is base run, blue is high NO_x regime, and red is low NO_x regime.